Preprints (www.preprints.org) | NOT PEER-REVIEWED | Posted: 19 July 2020 doi:10.20944/preprints202007.0406.v1

Peer-reviewed version available at *Appl. Sci.* **2020**, *10*, 5735; doi:10.3390/app10175735

Article

X-ray Photoelectron Spectroscopy for Determining Interface Dipoles of Self-Assembled Monolayers

Thomas C. Taucher [1], and Egbert Zojer [2,*]

[1] Institute of Solid State Physics, Graz University of Technology, NAWI Graz, Petersgasse 16, 8010 Graz, Austria; egbert.zojer@tugraz.at

* Correspondence: egbert.zojer@tugraz.at; Tel.: +43/316/873-8475

Featured Application: Authors are encouraged to provide a concise description of the specific application or a potential application of the work. This section is not mandatory.

Abstract: In the current manuscript we assess to what extent X-ray photoelectron spectroscopy is a suitable tool for probing the dipoles formed at interfaces between self-assembled monolayers and metal substrates. To that aim, we perform dispersion-corrected, slab-type band-structure calculations on a number of biphenyl-based systems bonded to a Au(111) surface via different docking groups. In addition to changing the docking chemistry (and the associated interface dipoles), also the impacts of polar tail-group substituents and varying dipole densities are investigated. We find that for densely-packed monolayers the shifts of the peak positions of the simulated XP-spectra are a direct measure for the interface dipoles. In the absence of polar tail-group substituents they also directly correlate with adsorption-induced work-function changes. At reduced dipole-densities this correlation deteriorates, as work function measurements probe the difference between the Fermi-level of the substrate and the electrostatic energy far above the interface, while core level shifts are determined by the local electrostatic energy in the region of the atom from which the photoelectron is excited.

Keywords: x-ray photoelectron spectroscopy, XPS, self-assembled monolayer, SAM, collective electrostatics, band-structure calculation, density-functional theory, DFT

1. Introduction

In the field of organic electronics, chemically bonded self-assembled monolayers (SAMs) have been used to change the electronic properties of a huge variety of interfaces.[1–18] They have allowed the realization of n-type organic transistors by screening interface traps,[3] they have been used to shift turn-on voltages of devices by several dozens of volts,[4–7] and they have been employed for tuning injection barriers, changing contact resistances by orders of magnitude.[8–18] Especially for the latter applications, the shift in the (electrostatic) energy landscape generated by the SAM is of crucial importance. On the one hand, this shift is a consequence of the intrinsic dipoles of the adsorbed molecules due to polar groups embedded into the molecular backbones[15,17,19–23] or due to polar tail-group substituents.[9,24–38] On the other hand, there is always an interface dipole localized in the immediate contact region between the substrate and the adsorbed molecule.[11,25,27,28,31,32,39–44] This interface dipole consists of the surface dipole of the (metal) substrate, the dipole associated with the (typically polar) docking group, and the bond dipole due to interfacial charge rearrangements following bond formation. The superposition of the electric fields due to the interface dipoles of all adsorbed molecules causes a step in the electrostatic energy.[31,40,42,45,46] This not only triggers a shift in the position of the vacuum level above the surface and, consequently, changes the sample work function;[8,11,14–17,19,21,22,27,28,31,32,35,41,43,44,47,39,25,48–52] it also modifies the interfacial energy-

© 2020 by the author(s). Distributed under a Creative Commons CC BY license.

Preprints (www.preprints.org) | NOT PEER-REVIEWED | Posted: 19 July 2020 doi:10.20944/preprints202007.0406.v1

Peer-reviewed version available at Appl. Sci. 2020, 10, 5735; doi:10.3390/app10175735

level alignment, i.e., the positions of the electronic states of the adsorbed monolayer relative to those of the substrate.[27,28,31,39,40,42,45–47,53–62] This has an immediate impact on charge-transport through the adsorbed layer[53–62] and also on the positions of the core levels of the adsorbate.[20–22,42,48,49,63–65]

These changes in core-level binding energies can be probed by X-ray photoelectron spectroscopy (XPS), [66–69] which is one of the default techniques for characterizing SAMs, used, for example, for analyzing the quality of self-assembled monolayers and to verify bonding.[70–81] In this paper we will argue that the electrostatic core-level shifts make XPS an ideally suited tool for probing interface dipoles. For supporting that claim, we will use state of the art quantum-mechanical simulations to determine core-level shifts encountered biphenyl-based SAMs attached to a Au(111) substrate by a variety of chemically different docking groups. To the best of our knowledge, a corresponding set of experimental XPS data with systematically varied docking groups and consistent film structures and morphologies does not exist yet. Nevertheless, first steps in that direction have been undertaken and biphenyl-based SAMs on all kinds of substrates have been studied.[72,80–88,60] We, however, do not consider this to be an all too serious problem, as we have high confidence in the employed computational approach, which is described in the following section. This confidence is based on the fact that in the past we have observed an excellent agreement between measured and simulated core-level shifts for a variety of self-assembled monolayers.[21,22,48,49,64,65]

2. Computational Methodology

The structural and electronic properties of the metal-SAM interfaces were simulated by density functional theory, DFT, employing the all-electron, full potential FHI-aims code version 190715[89–93] and periodic boundary conditions. The Perdew-Burke-Ernzerhof (PBE)[94,95] functional was used for describing exchange and correlation. Furthermore, long-range van der Waals interactions were accounted for by employing the surface version[96] of the Tkatchenko-Scheffler dispersion correction,[97] which was specifically parametrized for treating adsorbing molecules on metal substrates. The dispersion corrections between the Au atoms of the metal slab were turned off. All calculations were done with the so-called tight basis set for all atomic species (as supplied by FHI-aims). A thorough description of the corresponding basis functions is included in the Supporting Information. Reciprocal space was sampled by a converged Γ-centered 15×10×1 grid for the full coverage systems and by accordingly smaller sized grids for larger super cells. The change of the electron density was converged to 10^{-5} e^- and the total energy to 10^{-6} eV.

Interfaces were modelled employing the repeated-slab approach with the Au(111) substrate represented by five metal layers. The bottom three Au layers were kept fixed in all calculations to avoid spurious relaxations at the bottom surface. The periodic replicas of the slabs were quantum-mechanically and electrostatically decoupled by a vacuum gap of more than 20 Å and a self-consistent dipole correction.[98,99] The geometries of the adsorbate molecules and the top two Au-layers in the full coverage unit cells were fully relaxed until the remaining forces on each atom were below 10^{-3} eV/Å. The geometries of the other supercells considered here were directly derived from the full coverage unit cell by replicating it in x- and y-directions and removing all but one molecule from the resulting cell (see Supporting Information). These supercells were considered as model systems to study the impact of diluting the interfacial dipoles. Thus we fixed the remaining molecule in the geometry it adopts in the densely-packed layer, to prevent it from falling over.[100]

The change of the work function ($\Delta\Phi$) is defined as the difference of the calculated work functions at the bottom side of the Au(111)-slab (Φ_{Au} = 5.10 eV for all systems) and above the self-assembled monolayer. Furthermore, the work function change of VIa, i.e. the difference between the pristine Au(111) and the SAM moved 1 Å further away from its equilibrium adsorption distance, was defined as a reference point for all other calculations and amounts to $\Delta\Phi_{ref}$ = 0.11 eV.

The core-level binding energies were calculated using the initial state approach, relying on the Kohn-Sham eigenvalues of the respective orbitals. This approach does not provide absolute values

Preprints (www.preprints.org) | NOT PEER-REVIEWED | Posted: 19 July 2020 doi:10.20944/preprints202007.0406.v1

Peer-reviewed version available at Appl. Sci. 2020, 10, 5735; doi:10.3390/app10175735

of the core-level binding energies, but yields relative shifts between different systems.[63,68,101–106] We have also found it to provide a very good description of core-level shifts in SAMs.[21,22,48,49,64,65] In fact, when modelling the XP spectra of (partially) aromatic hydrocarbon SAMs bonded to Au substrates, we typically find that shifting the calculated spectra to higher binding energies by between 18.9 to 19.0 eV[22,49,107,108] yields an excellent correlation with experimental data. Therefore, throughout the manuscript work-function shifts relative to the peak position of the vacuum-level aligned system VIa are reported. The calculated value of that reference energy is -263.95 eV.

Another complication when employing the initial-state approach is that (in contrast to final-state approaches)[68,109–111] it does not account for core-hole screening effects. Unfortunately, final-state approaches are not applicable to systems like the ones considered here, as in conjunction with periodic boundary conditions one would need unit cells comprising thousands of atoms in order to avoid spurious collective electrostatic effects due to periodic replicas of the core holes (and the compensation charges).[64,112] Therefore, we resorted to an a posteriori correction of screening by the metal substrate relying on an image charge model, which is explained in detail in the Supporting Information.[113,114] In passing we note that screening by the metal substrate has only a comparably minor impact on the spectra shown below, as we are dealing with rather extended, upright standing molecules, whose spectra are dominated by excitations of atoms, which are rather far away from the substrate. To account for the finite escape depth of the photoelectrons from lower-lying atoms, we scaled their contributions by an exponential attenuation function[115] setting the incident photon energy to 580 eV, as described in detail in the Supporting Information. To obtain the final spectra, the discrete peaks were convoluted with a Gaussian function with a variance of 0.3 eV.

For the analysis and visual representation of the data, Python was used in combination with NumPy[116] and matplotlib[117]. Ovito[118] was applied for generating the 3D view of the systems and for the 2D potential plot we used VESTA.[119] Finally, the figures were compiled with GIMP.[120]

3. Results and Discussion

3.1. Energetics of a metal-SAM interface

For understanding the correlation between XP spectra and interface dipoles, it is useful to first consider how interface dipoles impact the electronic properties of a system consisting of an inorganic substrate and a chemically bonded monolayer (formed by upright-standing molecules). For the sake of simplicity, in the following we will focus on metal substrates. In this way, further complications due to band-bending effects[35,64,121,122] in semiconducting substrates (and their modification by the adsorbate layer) can be avoided.

Preprints (www.preprints.org) | NOT PEER-REVIEWED | Posted: 19 July 2020 doi:10.20944/preprints202007.0406.v1

Peer-reviewed version available at Appl. Sci. 2020, 10, 5735; doi:10.3390/app10175735

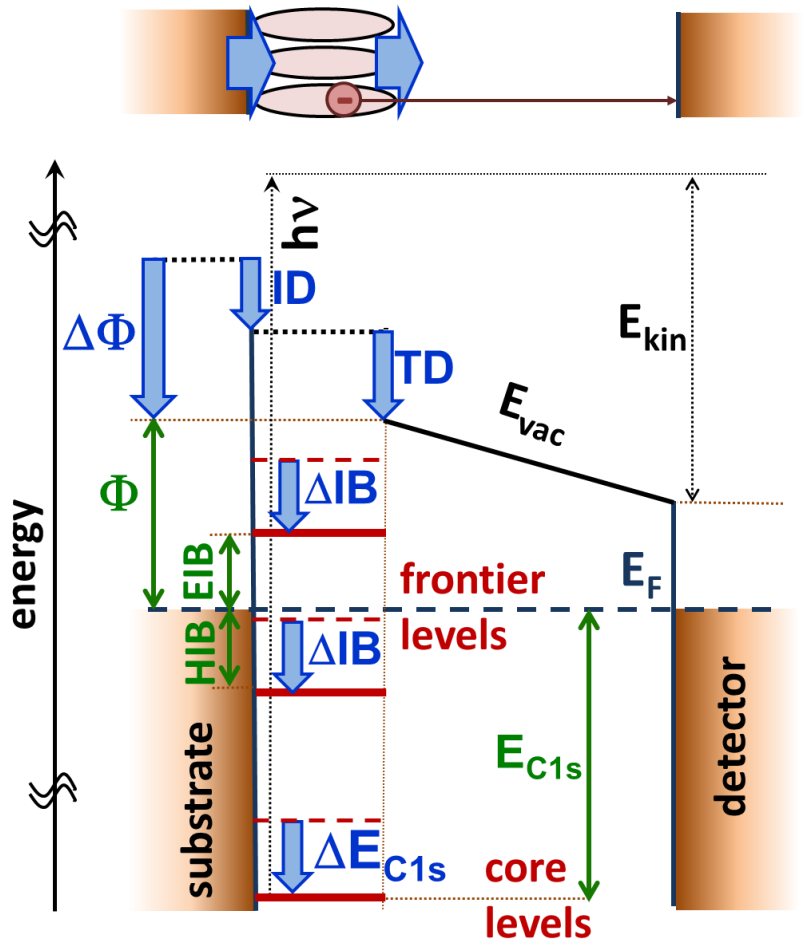

Figure 1: Schematics of the energy landscape of a metal-SAM interface and an XPS experiment (disregarding the bias voltage applied between substrate and detector). The interface electronic structure is characterized by the work function, Φ, by the alignment of the frontier levels determining electron- and hole-injection barriers, EIB and HIB, and by the energetic positions of the core levels, here exemplarily denoted as EC1s. The shift of the electrostatic energy due to the interface dipole, ID, determines the changes in the injection barriers, DIB, and the core-level shifts, DEC1s. The work-function change, DΦ, is additionally influenced by the energetic shift due to the tail-group dipole, TD. Absorption of an X-ray photon with energy hν creates a photoelectron, which at the position of the detector has a with kinetic energy Ekin. Additional positive potentials (not included in the plot) applied to the detector relative to the substrate increase the measured kinetic energy of the photoelectron. The top panel sketches the metal-SAM interface, whose properties are determined by the interface- and the tail-group dipole. In passing we note that the actual situation can be further complicated, when additional dipoles are contained along the backbones of the molecules.[15,17,19–22]

A schematic representation of the electronic structure of the metal-SAM interface is shown in Figure 1 for the case of a SAM in which an interface-dipole occurs (virtually all SAMs) and in which also a functional tail group is used bearing a tail-group dipole. Due to the superposition of the fields generated by the dipoles in the densely-packed monolayer (i.e., due to collective electrostatic effects),[27,31,40,42,45,46,64,123,124] steps in the electrostatic energy occur. The steps due to the interface dipole, ID, and due to the tail group dipole, TD, are indicated by vertical blue arrows. The sum of these two energy shifts causes the change in substrate work function due to monolayer adsorption, ΔΦ. Conversely, only the interface dipole is responsible for the change in injection barriers, ΔIB, which determines the final electron- and hole-injection barriers, EIB and HIB, respectively. The core levels are shifted in line with the frontier levels. Consequently, the interface

Preprints (www.preprints.org) | NOT PEER-REVIEWED | Posted: 19 July 2020 doi:10.20944/preprints202007.0406.v1

Peer-reviewed version available at Appl. Sci. 2020, 10, 5735; doi:10.3390/app10175735

dipole should result in a shift of the positions of the core levels relative to the Fermi-level of the substrate, ΔE_{C1s}, that is equivalent to ΔIB. This shift is directly translated into a modification of the kinetic energies of the electrons, E_{kin}, and, thus, in a shift of the XP spectra.

In this context it is important to stress that the above considerations disregard energetic shifts due to interfacial charge transfer processes, which could significantly modify the energies of strongly localized orbitals (i.e., the core levels). Indeed, for the atoms in a SAM that are in the immediate vicinity of the interface, this typically modify the core-level binding energies,[67–69,110,125,126] an effect that has also been observed for simulations on SAMs.[108] In experiments on extended, upright standing molecules it will, however, be inconsequential for the measured spectra, as the atoms in the immediate vicinity of the interface affected by these "chemical" shifts hardly contribute to the measured spectra. This is a consequence of the finite escape depth of the photoelectrons.

Finally, it should be mentioned that in the absence of an energetic shift due to a tail group dipole (or when comparing differently docked systems with identical tail-group dipoles), the above considerations imply that SAM-induced changes of the substrate work-function should directly correlate with shifts in core-level binding energies. Below, we will test under which circumstances such a situation is encountered at a metal-SAM interface.

3.2. Investigated Systems

To assess the possibility of probing bond dipoles by X-ray photoelectron spectroscopy, we simulated SAMs on Au(111) surfaces, as such systems have been studied extensively,[70,71,73,78,127] which qualifies them as prototypical model systems. As molecular backbones we chose biphenyls with two molecules per $(3 \times \sqrt{3})$*rect* surface unit cell arranged in a herringbone structure.[84] As docking groups we considered thiolates (system I),[70,71,73,78] methyl thiolates (system II),[70,71,73,78] pyridines (system III),[54,128–133] isocyanides (system IV)[39,133–135] and cyanides (system V). For the sake of comparison, we also simulated an upright-standing biphenyl layer not bearing a dedicated docking group (system VI) which represents a metastable structure, as the equilibrium configuration for the biphenyl-Au interface would very likely be flat-lying molecules. Due to different interfacial charge rearrangements and intrinsic dipole moments associated with the docking groups in these six systems, we expect distinct variations of the respective interface dipoles. Notably, in system VI, the only reason for an interface dipole would be Pauli-pushback.[47,136,137] To eliminate also that effect and to generate an essentially dipole-free interface, we also considered a system with the biphenyl layer shifted by 1 Å further away from the substrate (system VIa). In passing we note that increasing the distance from the substrate by yet another 1 Å does not change the spectrum (see Supporting Information). The electronic structure of system VIa is essentially identical to what is obtained when assuming vacuum-level alignment between a Au(111) surface and a free-standing biphenyl monolayer (the calculated work-function reduction is on the order of 0.1 eV; for further information see Supporting Information). Additionally, we considered two systems bearing electron accepting (system VII) and electron donating (system VIII) tail-group substituents. These are known to change the work function without affecting the alignment of the frontier levels.[27]

Preprints (www.preprints.org) | NOT PEER-REVIEWED | Posted: 19 July 2020 doi:10.20944/preprints202007.0406.v1

Peer-reviewed version available at Appl. Sci. 2020, 10, 5735; doi:10.3390/app10175735

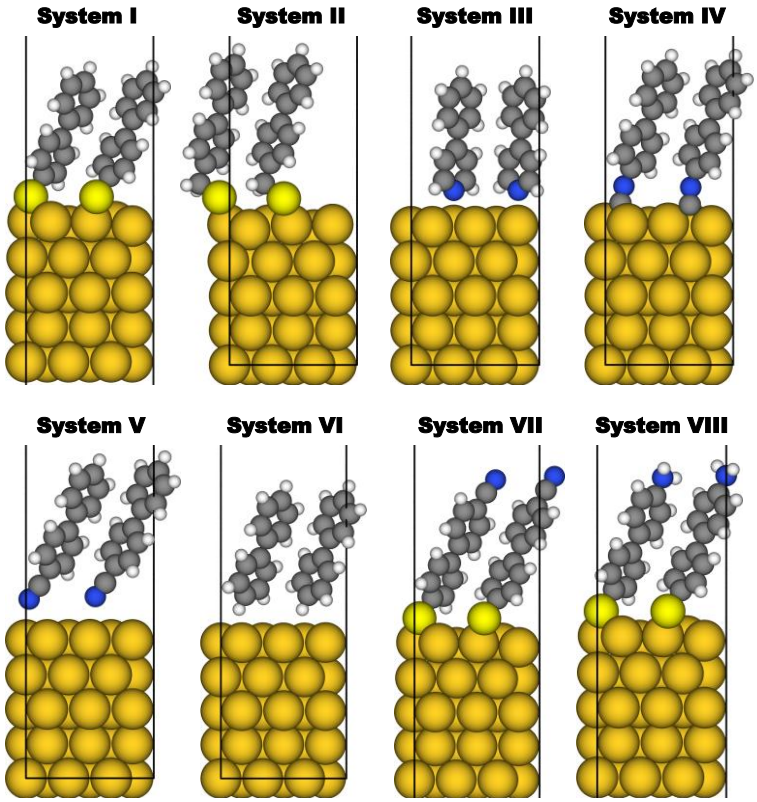

Figure 2. Front view of the unit cells investigated in the present study. The self-assembled monolayers are all derived from a biphenyl backbone and bear different docking groups (systems I to VI) or different tail groups (system VII and VIII). The SAMs are bonded to a Au(111) metal slab consisting of 5 layers of gold atoms. The docking groups comprise thiolate (system I), methyl-thiolate (system II), pyridine (system III), isocyanide (system IV) and cyanide (system V). System VI is an upright standing biphenyl layer not bearing any docking group. Systems VII and VIII are both bonded via thiolates, but contain different (polar) tail groups (a nitrile in the case of system VII and an amine in the case of system VIII). The molecules are arranged in a herringbone pattern, as can be seen in the top views of the unit cell shown in the Supporting Information. Color code: dark yellow: Au, bright yellow: S, grey: C, green: N, and white: H.

3.3. Calculated core-level binding energies, XP spectra, and work-function changes

3.3.1. Energetic shifts due to variations in the interface dipole

In Figure 3, we show the core-level binding energies and XP spectra of systems I, III, V, and VIa as prototypical examples for the impact of the docking groups on the core-level binding energies. In the following, the "vacuum level alignment" system VIa is used as energy reference for the work-function as well as for the core-level binding energies (for the absolute values of the reference energies see Methods section). This directly yields ΔE_{C1s} and $\Delta\Phi$ (i.e, the quantities shown in Figure 1). As far as the systems not displayed in Figure 3 are concerned, the data points for II essentially coincide with those of I and (apart from chemical shifts for the carbon atoms directly bonded to nitrogen atoms) the binding energies of III and V are also similar. System VI is similar to VIa with binding energies shifted to higher values by 0.34 eV. The corresponding data can be seen in the Supporting Information, where we show a (somewhat busy) plot analogous to Figure 3 containing values for all investigated systems. Compared to System VIa, the core-level binding energies in all chemically bonded SAMs are shifted to higher (more negative) binding energies by several eV. The effect is largest for III, for which the

Preprints (www.preprints.org) | NOT PEER-REVIEWED | Posted: 19 July 2020 doi:10.20944/preprints202007.0406.v1

Peer-reviewed version available at Appl. Sci. 2020, 10, 5735; doi:10.3390/app10175735

shift amounts to 2.8 eV (see black arrow). Even between docked systems, the peak positions vary by 1.6 eV with the smallest value (-265.2 eV) for the methyl thiolate and the largest (-266.8 eV) for the pyridine. This is exactly the situation one would expect according to Figure 1 for varying interface dipoles as a consequence of collective electrostatic effects.[31,40,45,46,64]

Superimposed on these electrostatic shifts of the XPS peaks, one can also identify the chemical shifts due to the differently bonded carbon atoms (cf. Figure 2a). For example, the carbon atoms connecting the two benzene rings are shifted by ~0.5 eV relative to the other carbon atoms of the rings. Also the carbon atoms attached to the docking groups are chemically shifted, resulting in distinct variations of the binding energies. This is, however, rather inconsequential for the positions and shapes of the XP spectra as a consequence of the finite escape depth of the photoelectrons. This is well visible, for example, for the isocyanide-docked SAM (system IV), where the lowest carbon atoms are shifted by ~2 eV relative to the ones in the rings. The latter still rather exclusively determine the position of the peak in the corresponding XP spectrum.

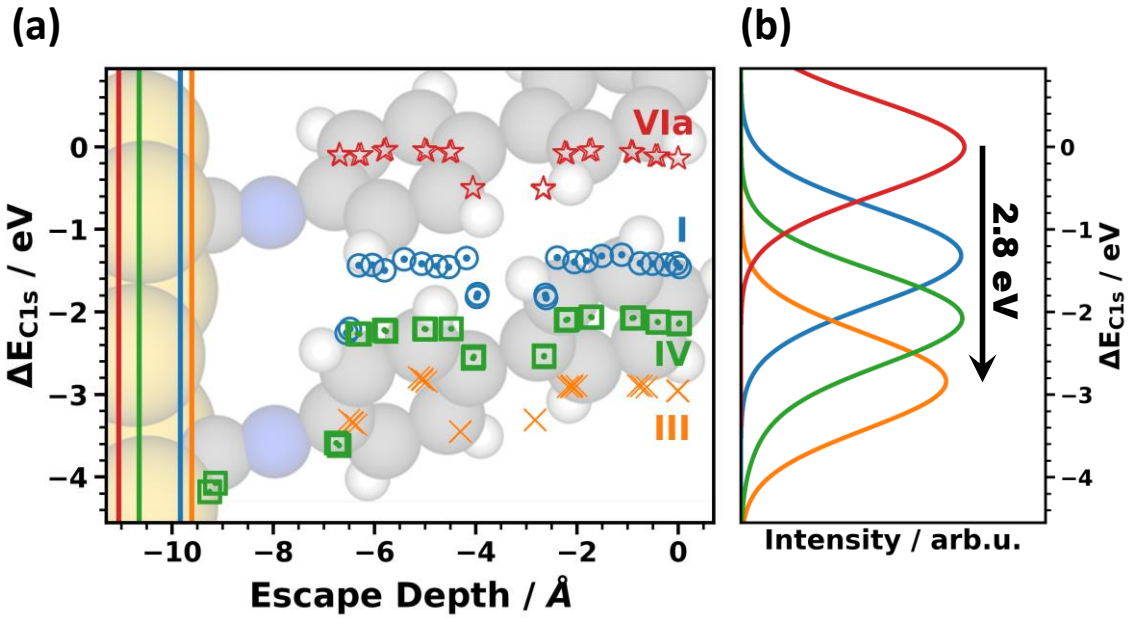

Figure 3. (a) Simulated shifts of carbon 1s orbital energies, DEC1s, as a function of the escape depth of the electrons for the prototypical systems I, III, IV, and VIa; (b) corresponding XP spectra generated from the calculated energy levels. The energies scale is chosen relative to the position of the peak in the XP spectrum for the vacuum-level aligned system VIa. The escape depth defined as the distance from the topmost carbon atom is chosen as the parameter on the x-axis considering that the highest atoms primarily determine the XP spectra. As the extent of the SAMs between the bottom ring and the metal substrate varies due to the different docking groups, this choice of the x-axis also largely aligns biphenyls in the different systems. System IV is shown in the background as an example of the structure of one of the SAMs considered in the plot. Due to the different SAM thicknesses, we included vertical lines in panel (a), which designate the positions of the centers of the atoms of the topmost Au layer. The large number of data points for each system is a consequence of the two inequivalent molecules per unit cell.

Provided that the primary core-level shifts are truly a consequence of collective electrostatic effects caused by interface dipoles they should directly correlate with the SAM-induced changes in the work function for systems I to VIa. To test that, we plotted $\Delta\Phi$ as a function of ΔE_{C1s} for all investigated SAMs in Figure 4. Indeed, the data for all SAMs without polar tail group substituents align perfectly along a straight line with a slope of 1 passing through the origin. This supports the assessment that in these systems core-level shifts and work-function changes have the same origin (namely the interface dipole). In passing we note that the dipole due to the terminal C-H bond of the

Preprints (www.preprints.org) | NOT PEER-REVIEWED | Posted: 19 July 2020 doi:10.20944/preprints202007.0406.v1

Peer-reviewed version available at Appl. Sci. 2020, 10, 5735; doi:10.3390/app10175735

biphenyl cancels out for the evolution of ΔΦ vs. ΔE_{C1s} (at least for similar coverages and tilt angles), as the non-interacting biphenyl monolayer is used as the reference for both quantities.

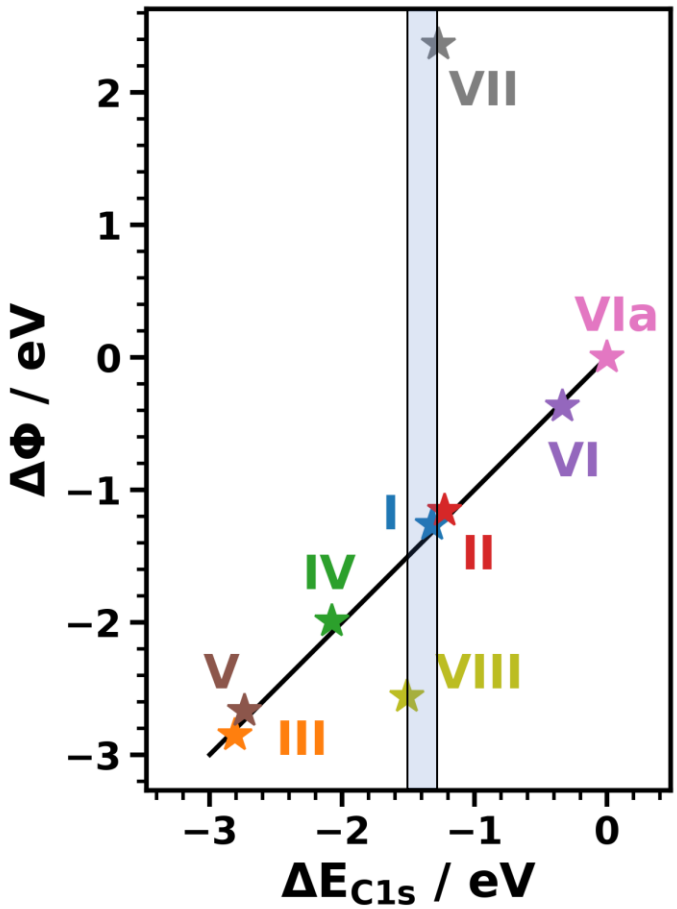

Figure 4: Correlation between the change in work function, DF, and the shift in binding energy,DEC1s, for all systems relative to system VIa (as non-interacting reference system in which no interface dipole occurs) The black line indicates a linear curve with a slope of 1 through the origin. The shaded area represents the range over which the values for DEC1s vary between systems I, VII, and VIII.

3.3.2. Influence of Different Tail Groups on the XP-spectra

This raises the question, what would happen if the SAM-forming molecules were substituted with tail-groups bearing dipoles significantly different from the terminal C-H bond of a phenyl ring. According to Figure 1, this should (significantly) modify the work-function shift, while leaving the core-level binding energies essentially unchanged, with the exception of chemical shifts experienced by carbon atoms in or directly bonded to the substituents. To test that hypothesis, we simulated systems VII and VIII containing -CN and -NH_2 tail groups. As far as the simulated core-level binding energies are concerned, we find them to be very similar for all three systems (I, VII, and VIII), as shown in Figure 5. Concerning the chemically shifted C1s binding energies of the uppermost carbon atoms, for system VII the shift of the top carbon atoms in the phenylene and the carbons in the -CN groups go in opposite directions. Thus their impacts on the XP spectrum essentially cancel. As a consequence, the peak position of the C1s XP spectra of I and VII are virtually the same. Also in VIII the shift of the peak remains comparably small (amounting to only 0.19 eV), as there only the topmost carbon atoms in the two molecules per unit cell are affected by the presence of the amine. This means

Preprints (www.preprints.org) | NOT PEER-REVIEWED | Posted: 19 July 2020 doi:10.20944/preprints202007.0406.v1

Peer-reviewed version available at Appl. Sci. 2020, 10, 5735; doi:10.3390/app10175735

that for all systems considered in the present study, the position of the peak in the C1s spectrum is a valid measure for the interface dipole.

As shown in Figure 4, in sharp contrast to the core-level spectra, the work-function changes for VII and VIII differ significantly from that of I (by 3.63 eV for VII and by -1.30 eV for VIII). This is again fully consistent with the model described in section 2.

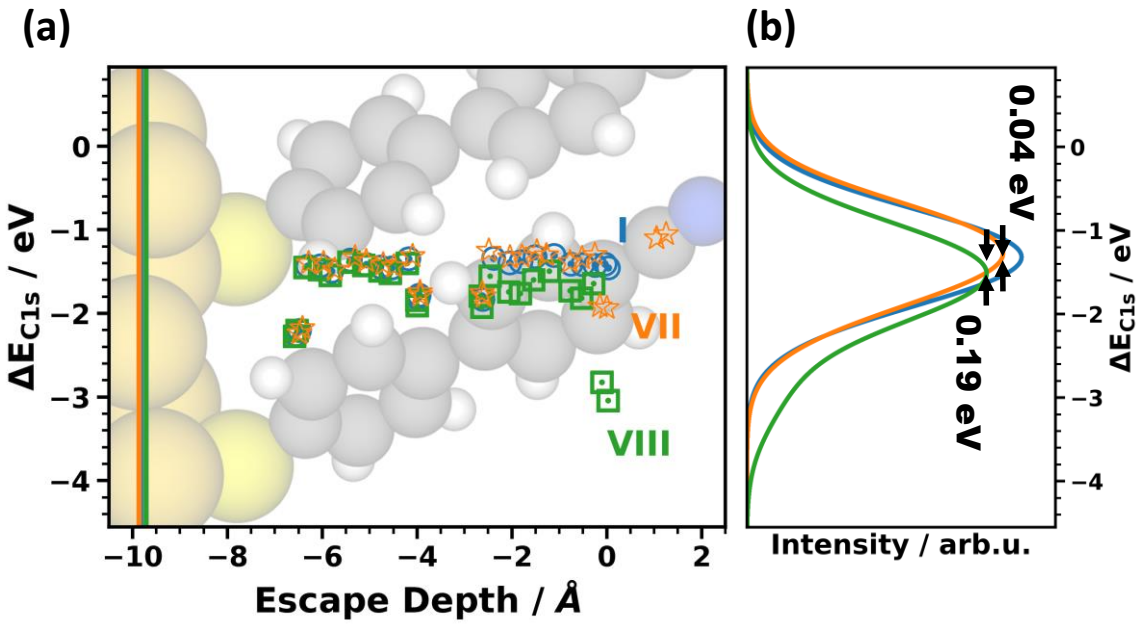

Figure 5. (a) Simulated shifts of carbon 1s orbital energies, DEC1s, as a function of the escape depth of the electrons for the equally docked systems I, VII, and VIII; (b) corresponding XP-spectra generated from the calculated energy levels. As the substituents significantly impact the extent of the SAMs above the top ring, but its volume density is rather low, the topmost carbon atom of the benzene ring was chosen as the origin of the x-axis. In this way, the axis is consistent with the x-axis of Figure 4 and the carbon rings are aligned at essentially the same positions. The large number of data points for each system is a consequence of the two inequivalent molecules per unit cell.

3.3.3. Coverage Dependence

As a last aspect it should be addressed to what extent the above conclusions hold for less densely packed polar layers at the interface.[42,113] To assess that, in a gedankenexperiment we constructed hypothetical low-coverage systems with upright-standing molecules (for details see Methods section and Supporting Information). Based on the Helmholtz solution to the Poisson equation, one would expect a linear dependence of the dipole density and, thus, of $\Delta\Phi$ and ΔE_{C1s} on coverage. The actual coverage-dependence of $\Delta\Phi$ and ΔE_{C1s} is shown in Figure 6 for the same systems that had already been considered in Figure 3. Interestingly, one observes that $\Delta\Phi$ changes much more strongly at low than at high coverages. This is a consequence of depolarization effects. These strongly reduce the interface dipoles at high coverages.[138–146] Therefore, work-function changes at full coverages are strongly reduced compared to what one would expect based on the dipoles associated with the adsorption of a single molecule.[147]

Preprints (www.preprints.org) | NOT PEER-REVIEWED | Posted: 19 July 2020 doi:10.20944/preprints202007.0406.v1

Peer-reviewed version available at Appl. Sci. 2020, 10, 5735; doi:10.3390/app10175735

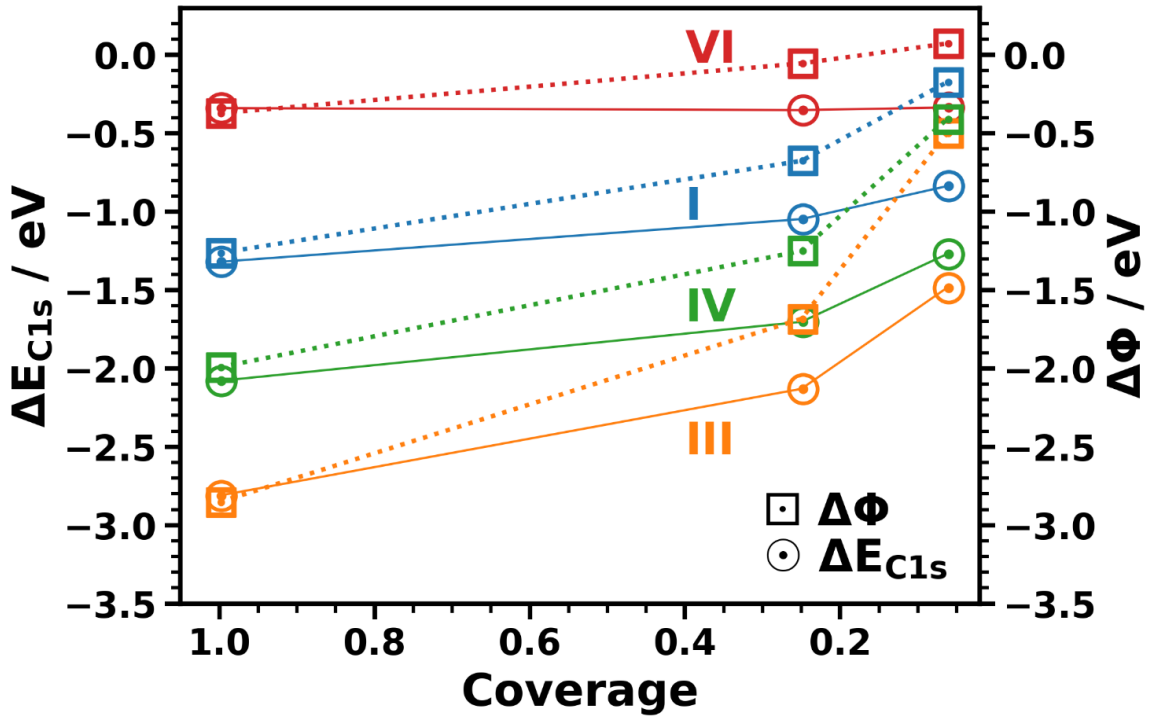

Figure 6: Core-level shift, DEC1s, (circles) and work-function change DF (square symbols) for systems I, III, IV, and VI as a function of coverage (varied between full, a quarter and 1/16 coverage, where the latter approaches the single molecule limit, see Supporting Information). All energies are reported relative to the values of the non-interacting reference system VIa.

Another observation in Figure 6 is that the coverage-dependence of the core-level binding energies (circles full line) is much weaker than that of ΔΦ (squares and dotted line). This is particularly obvious for system VI, for which there is almost no change of ΔE_{C1s} with coverage, while the work function still changes by ~0.5 eV. Qualitatively, the behavior is, however, the same for all studied systems, as shown in Figure 7. There, one sees that the energy range covered by the ΔΦ values is significantly larger than that for ΔE_{C1s}. As a result, the slope of the linear fit to the dependence of ΔΦ on ΔE_{C1s} (black lines in Figure 7) significantly decreases with decreasing coverage.

Preprints (www.preprints.org) | NOT PEER-REVIEWED | Posted: 19 July 2020 doi:10.20944/preprints202007.0406.v1

Peer-reviewed version available at Appl. Sci. 2020, 10, 5735; doi:10.3390/app10175735

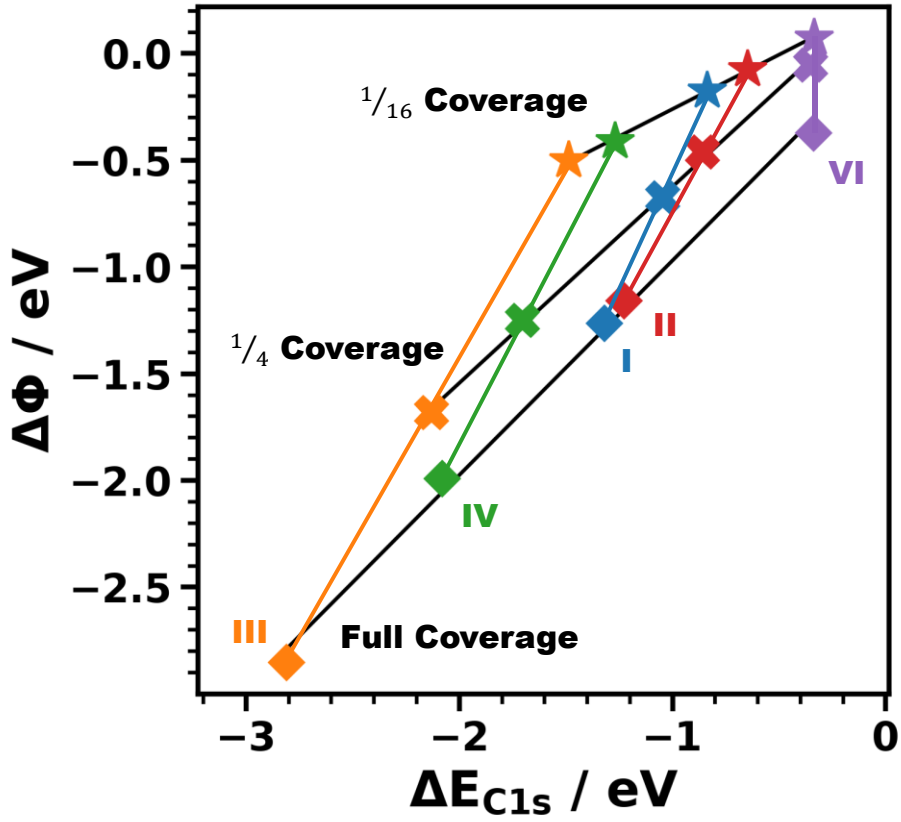

Figure 7. Core-level shift as a function of the work-function change for system I (blue), system II (red), system III (orange), system IV (green), and system V (violet). Results for full, ¼ and 1/16 coverage are compared. The black lines are fits to all systems for specific coverages, while the colored lines were fitted to the coverage-dependence for a specific system.

The main consequence of this observation is that at low dipole densities (in contrast to the full-coverage case, see above) ΔE_{C1s} is no longer a direct measure for the interface dipole. This can be explained by the different degrees of locality with which $\Delta\Phi$ and ΔE_{C1s} probe the electronic structure of the interface:[48,146,148] The value of $\Delta\Phi$ is determined by the energy difference between the Fermi level and the vacuum level far above the surface, i.e., in the far field. Conversely, core-level binding energies probe the electrostatic energy in the immediate vicinity of the atom whose core electron is excited.[47] The latter is comparably close to the interface dipole at the bond between the molecule and the substrate. Thus, the shift in the electrostatic energy due to the dipole is still relevant, even if it is strongly reduced due to the drop of the shift with the inverse of the third power of the distance between atom and dipole. This is illustrated in Figure 8, where we show the change in electrostatic energy due to the formation of the bond between the pyridine-docked SAM and the metal substrate. consequently, Figure 8 does not actually reflect the impact of the entire interface dipole, but only of the part resulting from the bond dipole. This quantity, can, however, be calculated conveniently by subtracting the electrostatic energies of the sub-systems from that of the bonded interface, which is not possible for the full interface dipole. It is also well suited to qualitatively illustrate the difference between the local and the far-field situation, even if one cannot expect quantitative agreement with the data from Figures 6 and 7, which are still determined by the entire interface dipole. For the full coverage system in the bottom panel of Figure 8, the main drop in electrostatic energy occurs at the immediate metal-pyridine interface and the electrostatic energy in the region of the top ring is essentially the same as far above the sample (despite a minor potential variation at the distance of the topmost C-H bond). Conversely, at 1/16 coverage the far-field electrostatic energy far above the interface (relevant for the work function) is several tenths of an eV higher than in the region of the upper carbon atoms (determining the position of the XPS peak).

Preprints (www.preprints.org) | NOT PEER-REVIEWED | Posted: 19 July 2020 doi:10.20944/preprints202007.0406.v1

Peer-reviewed version available at Appl. Sci. 2020, 10, 5735; doi:10.3390/app10175735

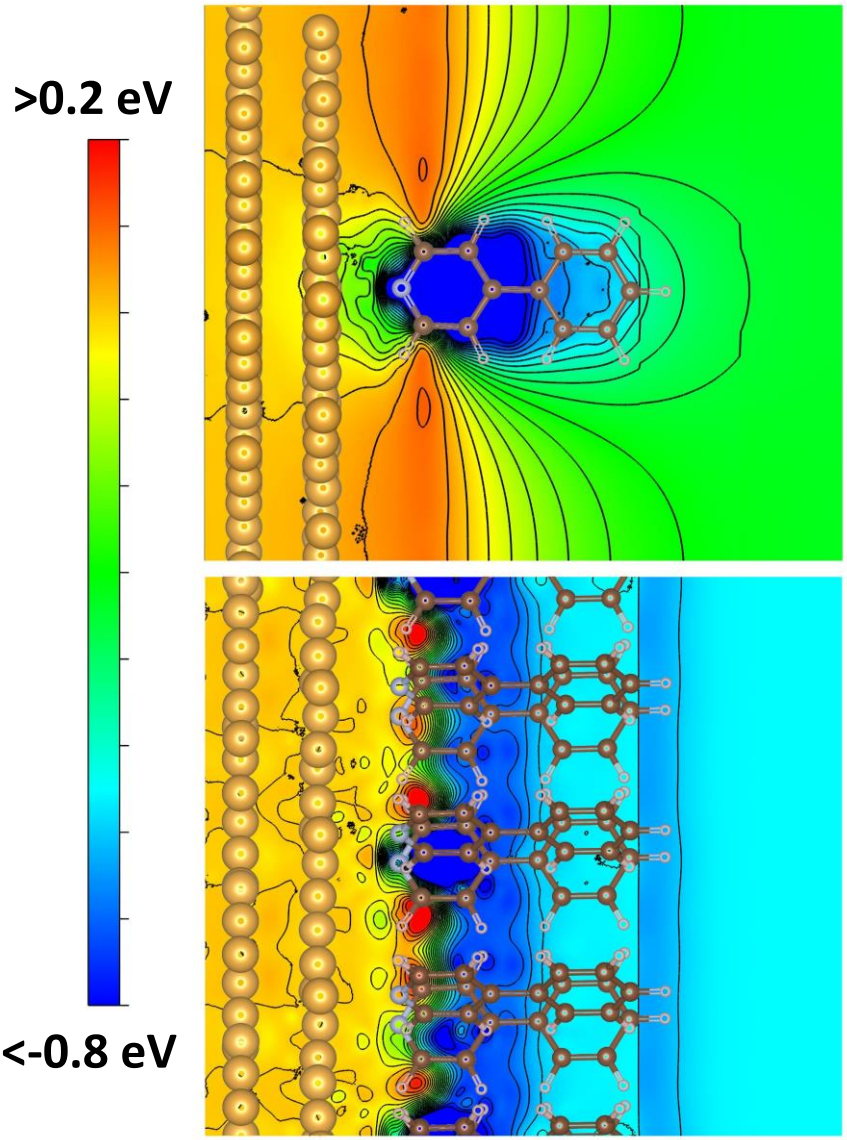

Figure 8. Contour plot of the change in the electrostatic energy due to metal-SAM bonding, i.e., due to the bond dipole (as part of the interface dipole) for system III. The potential is plotted for a plane defined by the plane of one of the molecules in the unit cell (see Supporting Information. The top (bottom) panel contains the result for 1/16 (full) coverage. Isolines are shown in steps of 0.05 eV.

4. Conclusions

In the present contribution it is shown that X-ray photoelectron spectroscopy is a suitable tool for determining interface dipoles in densely-packed self-assembled monolayers. This is shown via simulations on a number of biphenyl-based monolayers bonded to a Au(111)-substrate by a broad range of different docking groups. The varying interface dipoles in these systems result in shifts of the core-level binding energies by more than one eV, concomitantly shifting also the associated XP spectra. For SAMs not bearing polar tail groups the electrostatically triggered core-level shifts directly correlate with SAM-induced work-function changes. This correlation is broken, when work functions are further modified by polar tail-group substituents. Nevertheless, even in these cases the XP spectra are a direct measure for the interface dipoles. The situation changes, when the dipole density at the interface is reduced. Then core-level binding energies are still determined by the local electrostatic

Preprints (www.preprints.org) | NOT PEER-REVIEWED | Posted: 19 July 2020 doi:10.20944/preprints202007.0406.v1

Peer-reviewed version available at Appl. Sci. 2020, 10, 5735; doi:10.3390/app10175735

energy at the atoms from which the photoelectrons are excited. This energy is, however, no longer directly representative of the magnitude of the interface dipole, as it is strongly influenced, for example, by the distance of the excited atom from the location of the dipole. As a result, also the direct equivalence between core-level shifts and work-function changes is lost at reduced coverages, even though XPS still is suited for probing the local electrostatic energy (at least as long as chemical shifts, e.g., due to interfacial charge transfer are not superimposed on the electrostatic ones).

Supplementary Materials: Additional information on the computational methodology, additional computational results and views of unit cells and supercells are available online at www.mdpi.com/xxx/s1.

Author Contributions: Thomas Taucher has performed all calculations, analyzed the results, compiled most figures, and wrote a first draft of the manuscript. Egbert Zojer, guided and supervised the research, contributed to the analysis of the data, compiled Figure 1, and revised the manuscript.

Funding: This research was funded by the Austrian Science Fund (FWF): P28051-N36. The quantum mechanical calculations have been performed using the Vienna Scientific Cluster (VSC3).

Conflicts of Interest: The authors declare no conflict of interest.

References

1. Casalini, S.; Bortolotti, C.A.; Leonardi, F.; Biscarini, F. Self-assembled monolayers in organic electronics. *Chemical Society Reviews* **2017**, *46*, 40–71, doi:10.1039/C6CS00509H.
2. Halik, M.; Hirsch, A. The Potential of Molecular Self-Assembled Monolayers in Organic Electronic Devices. *Advanced Materials* **2011**, *23*, 2689–2695, doi:10.1002/adma.201100337.
3. Chua, L.-L.; Zaumseil, J.; Chang, J.-F.; Ou, E.C.-W.; Ho, P.K.-H.; Sirringhaus, H.; Friend, R.H. General observation of n-type field-effect behaviour in organic semiconductors. *Nature* **2005**, *434*, 194–199, doi:10.1038/nature03376.
4. Kobayashi, S.; Nishikawa, T.; Takenobu, T.; Mori, S.; Shimoda, T.; Mitani, T.; Shimotani, H.; Yoshimoto, N.; Ogawa, S.; Iwasa, Y. Control of carrier density by self-assembled monolayers in organic field-effect transistors. *Nature Materials* **2004**, *3*, 317–322, doi:10.1038/nmat1105.
5. Pernstich, K.P.; Haas, S.; Oberhoff, D.; Goldmann, C.; Gundlach, D.J.; Batlogg, B.; Rashid, A.N.; Schitter, G. Threshold voltage shift in organic field effect transistors by dipole monolayers on the gate insulator. *Journal of Applied Physics* **2004**, *96*, 6431–6438, doi:10.1063/1.1810205.
6. Pacher, P.; Lex, A.; Proschek, V.; Etschmaier, H.; Tchernychova, E.; Sezen, M.; Scherf, U.; Grogger, W.; Trimmel, G.; Slugovc, C.; et al. Chemical Control of Local Doping in Organic Thin-Film Transistors: From Depletion to Enhancement. *Advanced Materials* **2008**, *20*, 3143–3148, doi:10.1002/adma.200800058.
7. Aghamohammadi, M.; Rödel, R.; Zschieschang, U.; Ocal, C.; Boschker, H.; Weitz, R.T.; Barrena, E.; Klauk, H. Threshold-Voltage Shifts in Organic Transistors Due to Self-Assembled Monolayers at the Dielectric: Evidence for Electronic Coupling and Dipolar Effects. *ACS Appl. Mater. Interfaces* **2015**, *7*, 22775–22785, doi:10.1021/acsami.5b02747.

Preprints (www.preprints.org) | NOT PEER-REVIEWED | Posted: 19 July 2020 doi:10.20944/preprints202007.0406.v1

Peer-reviewed version available at Appl. Sci. 2020, 10, 5735; doi:10.3390/app10175735

8. Campbell, I.H.; Rubin, S.; Zawodzinski, T.A.; Kress, J.D.; Martin, R.L.; Smith, D.L.; Barashkov, N.N.; Ferraris, J.P. Controlling Schottky energy barriers in organic electronic devices using self-assembled monolayers. *Physical Review B* **1996**, *54*, R14321–R14324, doi:10.1103/PhysRevB.54.R14321.
9. Campbell, I.H.; Kress, J.D.; Martin, R.L.; Smith, D.L.; Barashkov, N.N.; Ferraris, J.P. Controlling charge injection in organic electronic devices using self-assembled monolayers. *Applied Physics Letters* **1997**, *71*, 3528–3530, doi:10.1063/1.120381.
10. Yan, H.; Huang, Q.; Cui, J.; Veinot, J.G.C.; Kern, M.M.; Marks, T.J. High-Brightness Blue Light-Emitting Polymer Diodes via Anode Modification Using a Self-Assembled Monolayer. *Advanced Materials* **2003**, *15*, 835–838, doi:10.1002/adma.200304585.
11. de Boer, B.; Hadipour, A.; Mandoc, M.M.; van Woudenbergh, T.; Blom, P.W.M. Tuning of Metal Work Functions with Self-Assembled Monolayers. *Advanced Materials* **2005**, *17*, 621–625, doi:10.1002/adma.200401216.
12. Jang, Y.; Cho, J.H.; Kim, D.H.; Park, Y.D.; Hwang, M.; Cho, K. Effects of the permanent dipoles of self-assembled monolayer-treated insulator surfaces on the field-effect mobility of a pentacene thin-film transistor. *Applied Physics Letters* **2007**, *90*, 132104, doi:10.1063/1.2457776.
13. Kitamura, M.; Kuzumoto, Y.; Kang, W.; Aomori, S.; Arakawa, Y. High conductance bottom-contact pentacene thin-film transistors with gold-nickel adhesion layers. *Appl. Phys. Lett.* **2010**, *97*, 033306, doi:10.1063/1.3465735.
14. Schulz, P.; Schäfer, T.; Zangmeister, C.D.; Effertz, C.; Meyer, D.; Mokros, D.; Zee, R.D. van; Mazzarello, R.; Wuttig, M. A New Route to Low Resistance Contacts for Performance-Enhanced Organic Electronic Devices. *Advanced Materials Interfaces* **2014**, *1*, 1300130, doi:10.1002/admi.201300130.
15. Kim, J.; Rim, Y.S.; Liu, Y.; Serino, A.C.; Thomas, J.C.; Chen, H.; Yang, Y.; Weiss, P.S. Interface Control in Organic Electronics Using Mixed Monolayers of Carboranethiol Isomers. *Nano Letters* **2014**, *14*, 2946–2951, doi:10.1021/nl501081q.
16. Fenwick, O.; Van Dyck, C.; Murugavel, K.; Cornil, D.; Reinders, F.; Haar, S.; Mayor, M.; Cornil, J.; Samorì, P. Modulating the charge injection in organic field-effect transistors: fluorinated oligophenyl self-assembled monolayers for high work function electrodes. *Journal of Materials Chemistry C* **2015**, *3*, 3007–3015, doi:10.1039/C5TC00243E.
17. Petritz, A.; Krammer, M.; Sauter, E.; Gärtner, M.; Nascimbeni, G.; Schrode, B.; Fian, A.; Gold, H.; Cojocaru, A.; Karner-Petritz, E.; et al. Embedded Dipole Self-Assembled Monolayers for Contact Resistance Tuning in p-Type and n-Type Organic Thin Film Transistors and Flexible Electronic Circuits. *Advanced Functional Materials* **2018**, *28*, 1804462, doi:10.1002/adfm.201804462.
18. Borchert, J.W.; Peng, B.; Letzkus, F.; Burghartz, J.N.; Chan, P.K.L.; Zojer, K.; Ludwigs, S.; Klauk, H. Small contact resistance and high-frequency operation of flexible low-voltage inverted coplanar organic transistors. *Nature Communications* **2019**, *10*, doi:10.1038/s41467-019-09119-8.
19. Evans, S.D.; Urankar, E.; Ulman, A.; Ferris, N. Self-assembled monolayers of alkanethiols containing a polar aromatic group: effects of the dipole position on

Preprints (www.preprints.org) | NOT PEER-REVIEWED | Posted: 19 July 2020 doi:10.20944/preprints202007.0406.v1

Peer-reviewed version available at Appl. Sci. 2020, 10, 5735; doi:10.3390/app10175735

molecular packing, orientation, and surface wetting properties. *J. Am. Chem. Soc.* **1991**, *113*, 4121–4131, doi:10.1021/ja00011a010.

20. Cabarcos, O.M.; Shaporenko, A.; Weidner, T.; Uppili, S.; Dake, L.S.; Zharnikov, M.; Allara, D.L. Physical and Electronic Structure Effects of Embedded Dipoles in Self-Assembled Monolayers: Characterization of Mid-Chain Ester Functionalized Alkanethiols on Au{111}. *The Journal of Physical Chemistry C* **2008**, *112*, 10842–10854, doi:10.1021/jp801618j.
21. Abu-Husein, T.; Schuster, S.; Egger, D.A.; Kind, M.; Santowski, T.; Wiesner, A.; Chiechi, R.; Zojer, E.; Terfort, A.; Zharnikov, M. The Effects of Embedded Dipoles in Aromatic Self-Assembled Monolayers. *Advanced Functional Materials* **2015**, *25*, 3943–3957, doi:10.1002/adfm.201500899.
22. Gärtner, M.; Sauter, E.; Nascimbeni, G.; Wiesner, A.; Kind, M.; Werner, P.; Schuch, C.; Abu-Husein, T.; Asyuda, A.; Bats, J.W.; et al. Self-Assembled Monolayers with Distributed Dipole Moments Originating from Bipyrimidine Units. *J. Phys. Chem. C* **2020**, *124*, 504–519, doi:10.1021/acs.jpcc.9b08835.
23. Baghbanzadeh, M.; Belding, L.; Yuan, L.; Park, J.; Al-Sayah, M.H.; Bowers, C.M.; Whitesides, G.M. Dipole-Induced Rectification Across Ag^{TS}/SAM//Ga_2O_3/EGaIn Junctions. *J. Am. Chem. Soc.* **2019**, *141*, 8969–8980, doi:10.1021/jacs.9b02891.
24. Kang, J.F.; Ulman, A.; Liao, S.; Jordan, R. Mixed Self-Assembled Monolayers of Highly Polar Rigid Biphenyl Thiols. *Langmuir* **1999**, *15*, 2095–2098, doi:10.1021/la9813883.
25. Zehner, R.W.; Parsons, B.F.; Hsung, R.P.; Sita, L.R. Tuning the Work Function of Gold with Self-Assembled Monolayers Derived from $X-[C_6H_4-C{:}C-]_n C_6H_4-SH$ (n = 0, 1, 2; X = H, F, CH_3, CF_3, and OCH_3). *Langmuir* **1999**, *15*, 1121–1127, doi:10.1021/la981114f.
26. Ganzorig, C.; Kwak, K.-J.; Yagi, K.; Fujihira, M. Fine tuning work function of indium tin oxide by surface molecular design: Enhanced hole injection in organic electroluminescent devices. *Appl. Phys. Lett.* **2001**, *79*, 272–274, doi:10.1063/1.1384896.
27. Heimel, G.; Romaner, L.; Brédas, J.-L.; Zojer, E. Interface Energetics and Level Alignment at Covalent Metal-Molecule Junctions: π-Conjugated Thiols on Gold. *Physical Review Letters* **2006**, *96*, doi:10.1103/PhysRevLett.96.196806.
28. Sun, Q.; Selloni, A. Interface and Molecular Electronic Structure vs Tunneling Characteristics of CH_3- and CF_3-Terminated Thiol Monolayers on Au(111). *J. Phys. Chem. A* **2006**, *110*, 11396–11400, doi:10.1021/jp064905w.
29. Yip, H.-L.; Hau, S.K.; Baek, N.S.; Ma, H.; Jen, A.K.-Y. Polymer Solar Cells That Use Self-Assembled-Monolayer- Modified ZnO/Metals as Cathodes. *Advanced Materials* **2008**, *20*, 2376–2382, doi:10.1002/adma.200703050.
30. Demirkan, K.; Mathew, A.; Weiland, C.; Yao, Y.; Rawlett, A.M.; Tour, J.M.; Opila, R.L. Energy level alignment at organic semiconductor/metal interfaces: Effect of polar self-assembled monolayers at the interface. *The Journal of Chemical Physics* **2008**, *128*, 074705, doi:10.1063/1.2832306.

Preprints (www.preprints.org) | NOT PEER-REVIEWED | Posted: 19 July 2020 doi:10.20944/preprints202007.0406.v1

Peer-reviewed version available at Appl. Sci. 2020, 10, 5735; doi:10.3390/app10175735

31. Heimel, G.; Romaner, L.; Zojer, E.; Bredas, J.-L. The Interface Energetics of Self-Assembled Monolayers on Metals. *Accounts of Chemical Research* **2008**, *41*, 721–729, doi:10.1021/ar700284q.
32. Malicki, M.; Guan, Z.; Ha, S.D.; Heimel, G.; Barlow, S.; Rumi, M.; Kahn, A.; Marder, S.R. Preparation and Characterization of 4′-Donor Substituted Stilbene-4-thiolate Monolayers and Their Influence on the Work Function of Gold. *Langmuir* **2009**, *25*, 7967–7975, doi:10.1021/la9004104.
33. Yoon, H.J.; Bowers, C.M.; Baghbanzadeh, M.; Whitesides, G.M. The Rate of Charge Tunneling Is Insensitive to Polar Terminal Groups in Self-Assembled Monolayers in $Ag^{TS}S(CH_2)_n M(CH_2)_m T//Ga_2O_3$/EGaIn Junctions. *J. Am. Chem. Soc.* **2014**, *136*, 16–19, doi:10.1021/ja409771u.
34. Lee, H.J.; Jamison, A.C.; Lee, T.R. Surface Dipoles: A Growing Body of Evidence Supports Their Impact and Importance. *Accounts of Chemical Research* **2015**, *48*, 3007–3015, doi:10.1021/acs.accounts.5b00307.
35. Vilan, A.; Cahen, D. Chemical Modification of Semiconductor Surfaces for Molecular Electronics. *Chemical Reviews* **2017**, *117*, 4624–4666, doi:10.1021/acs.chemrev.6b00746.
36. Lindell, L.; Vahlberg, C.; Uvdal, K.; Fahlman, M.; Braun, S. Self-assembled monolayer engineered interfaces: Energy level alignment tuning through chain length and end-group polarity. *Journal of Electron Spectroscopy and Related Phenomena* **2015**, *204*, 140–144, doi:10.1016/j.elspec.2015.04.006.
37. MacLeod, B.A.; Horwitz, N.E.; Ratcliff, E.L.; Jenkins, J.L.; Armstrong, N.R.; Giordano, A.J.; Hotchkiss, P.J.; Marder, S.R.; Campbell, C.T.; Ginger, D.S. Built-In Potential in Conjugated Polymer Diodes with Changing Anode Work Function: Interfacial States and Deviation from the Schottky–Mott Limit. *J. Phys. Chem. Lett.* **2012**, *3*, 1202–1207, doi:10.1021/jz300283h.
38. Schmidt, C.; Witt, A.; Witte, G. Tailoring the Cu(100) Work Function by Substituted Benzenethiolate Self-Assembled Monolayers. *The Journal of Physical Chemistry A* **2011**, *115*, 7234–7241, doi:10.1021/jp200328r.
39. Heimel, G.; Romaner, L.; Zojer, E.; Brédas, J.-L. Toward Control of the Metal−Organic Interfacial Electronic Structure in Molecular Electronics: A First-Principles Study on Self-Assembled Monolayers of π-Conjugated Molecules on Noble Metals. *Nano Letters* **2007**, *7*, 932–940, doi:10.1021/nl0629106.
40. Natan, A.; Kronik, L.; Haick, H.; Tung, R.T. Electrostatic Properties of Ideal and Non-ideal Polar Organic Monolayers: Implications for Electronic Devices. *Advanced Materials* **2007**, *19*, 4103–4117, doi:10.1002/adma.200701681.
41. Wang, L.; M. Rangger, G.; Ma, Z.; Li, Q.; Shuai, Z.; Zojer, E.; Heimel, G. Is there a Au–S bond dipole in self-assembled monolayers on gold? *Physical Chemistry Chemical Physics* **2010**, *12*, 4287–4290, doi:10.1039/B924306M.
42. Zojer, E.; Taucher, T.C.; Hofmann, O.T. The Impact of Dipolar Layers on the Electronic Properties of Organic/Inorganic Hybrid Interfaces. *Adv. Mater. Interfaces* **2019**, *6*, 1900581, doi:10.1002/admi.201900581.

Preprints (www.preprints.org) | NOT PEER-REVIEWED | Posted: 19 July 2020 doi:10.20944/preprints202007.0406.v1

Peer-reviewed version available at Appl. Sci. 2020, 10, 5735; doi:10.3390/app10175735

43. Alloway, D.M.; Hofmann, M.; Smith, D.L.; Gruhn, N.E.; Graham, A.L.; Colorado, R.; Wysocki, V.H.; Lee, T.R.; Lee, P.A.; Armstrong, N.R. Interface Dipoles Arising from Self-Assembled Monolayers on Gold: UV-Photoemission Studies of Alkanethiols and Partially Fluorinated Alkanethiols. 10.
44. Rusu, P.C.; Brocks, G. Surface Dipoles and Work Functions of Alkylthiolates and Fluorinated Alkylthiolates on Au(111). *The Journal of Physical Chemistry B* **2006**, *110*, 22628–22634, doi:10.1021/jp0642847.
45. Cahen, D.; Naaman, R.; Vager, Z. The Cooperative Molecular Field Effect. *Advanced Functional Materials* **2005**, *15*, 1571–1578, doi:10.1002/adfm.200500187.
46. Monti, O.L.A. Understanding Interfacial Electronic Structure and Charge Transfer: An Electrostatic Perspective. *The Journal of Physical Chemistry Letters* **2012**, *3*, 2342–2351, doi:10.1021/jz300850x.
47. Ishii, H.; Sugiyama, K.; Ito, E.; Seki, K. Energy Level Alignment and Interfacial Electronic Structures at Organic/Metal and Organic/Organic Interfaces. *Advanced Materials* **1999**, *11*, 605–625, doi:10.1002/(SICI)1521-4095(199906)11:8<605::AID-ADMA605>3.0.CO;2-Q.
48. Hehn, I.; Schuster, S.; Wächter, T.; Abu-Husein, T.; Terfort, A.; Zharnikov, M.; Zojer, E. Employing X-ray Photoelectron Spectroscopy for Determining Layer Homogeneity in Mixed Polar Self-Assembled Monolayers. *The Journal of Physical Chemistry Letters* **2016**, *7*, 2994–3000, doi:10.1021/acs.jpclett.6b01096.
49. Gärtner, M.; Sauter, E.; Nascimbeni, G.; Petritz, A.; Wiesner, A.; Kind, M.; Abu-Husein, T.; Bolte, M.; Stadlober, B.; Zojer, E.; et al. Understanding the Properties of Tailor-Made Self-Assembled Monolayers with Embedded Dipole Moments for Interface Engineering. *J. Phys. Chem. C* **2018**, *122*, 28757–28774, doi:10.1021/acs.jpcc.8b09440.
50. Braun, S.; Salaneck, W.R.; Fahlman, M. Energy-Level Alignment at Organic/Metal and Organic/Organic Interfaces. *Advanced Materials* **2009**, *21*, 1450–1472, doi:10.1002/adma.200802893.
51. Venkataraman, N.V.; Zürcher, S.; Rossi, A.; Lee, S.; Naujoks, N.; Spencer, N.D. Spatial Tuning of the Metal Work Function by Means of Alkanethiol and Fluorinated Alkanethiol Gradients. *The Journal of Physical Chemistry C* **2009**, *113*, 5620–5628, doi:10.1021/jp809156a.
52. Lange, I.; Reiter, S.; Pätzel, M.; Zykov, A.; Nefedov, A.; Hildebrandt, J.; Hecht, S.; Kowarik, S.; Wöll, C.; Heimel, G.; et al. Tuning the Work Function of Polar Zinc Oxide Surfaces using Modified Phosphonic Acid Self-Assembled Monolayers. *Advanced Functional Materials* **2014**, *24*, 7014–7024, doi:10.1002/adfm.201401493.
53. Kim, B.; Choi, S.H.; Zhu, X.-Y.; Frisbie, C.D. Molecular Tunnel Junctions Based on π-Conjugated Oligoacene Thiols and Dithiols between Ag, Au, and Pt Contacts: Effect of Surface Linking Group and Metal Work Function. *J. Am. Chem. Soc.* **2011**, *133*, 19864–19877, doi:10.1021/ja207751w.
54. Kim, T.; Darancet, P.; Widawsky, J.R.; Kotiuga, M.; Quek, S.Y.; Neaton, J.B.; Venkataraman, L. Determination of Energy Level Alignment and Coupling Strength

Preprints (www.preprints.org) | NOT PEER-REVIEWED | Posted: 19 July 2020 doi:10.20944/preprints202007.0406.v1

Peer-reviewed version available at Appl. Sci. 2020, 10, 5735; doi:10.3390/app10175735

in 4,4′-Bipyridine Single-Molecule Junctions. *Nano Lett.* **2014**, *14*, 794–798, doi:10.1021/nl404143v.

55. Egger, D.A.; Rissner, F.; Zojer, E.; Heimel, G. Polarity Switching of Charge Transport and Thermoelectricity in Self-Assembled Monolayer Devices. *Advanced Materials* **2012**, *24*, 4403–4407, doi:10.1002/adma.201200872.
56. Egger, D.A.; Liu, Z.-F.; Neaton, J.B.; Kronik, L. Reliable Energy Level Alignment at Physisorbed Molecule–Metal Interfaces from Density Functional Theory. *Nano Letters* **2015**, *15*, 2448–2455, doi:10.1021/nl504863r.
57. Obersteiner, V.; Egger, D.A.; Heimel, G.; Zojer, E. Impact of Collective Electrostatic Effects on Charge Transport through Molecular Monolayers. *J. Phys. Chem. C* **2014**, *118*, 22395–22401, doi:10.1021/jp5084955.
58. Obersteiner, V.; Huhs, G.; Papior, N.; Zojer, E. Unconventional Current Scaling and Edge Effects for Charge Transport through Molecular Clusters. *Nano Letters* **2017**, *17*, 7350–7357, doi:10.1021/acs.nanolett.7b03066.
59. Xie, Z.; Bâldea, I.; Smith, C.E.; Wu, Y.; Frisbie, C.D. Experimental and Theoretical Analysis of Nanotransport in Oligophenylene Dithiol Junctions as a Function of Molecular Length and Contact Work Function. *ACS Nano* **2015**, *9*, 8022–8036, doi:10.1021/acsnano.5b01629.
60. Xie, Z.; Bâldea, I.; Frisbie, C.D. Determination of Energy-Level Alignment in Molecular Tunnel Junctions by Transport and Spectroscopy: Self-Consistency for the Case of Oligophenylene Thiols and Dithiols on Ag, Au, and Pt Electrodes. *J. Am. Chem. Soc.* **2019**, *141*, 3670–3681, doi:10.1021/jacs.8b13370.
61. Xie, Z.; Bâldea, I.; Frisbie, C.D. Energy Level Alignment in Molecular Tunnel Junctions by Transport and Spectroscopy: Self-Consistency for the Case of Alkyl Thiols and Dithiols on Ag, Au, and Pt Electrodes. *J. Am. Chem. Soc.* **2019**, *141*, 18182–18192, doi:10.1021/jacs.9b08905.
62. Vilan, A.; Aswal, D.; Cahen, D. Large-Area, Ensemble Molecular Electronics: Motivation and Challenges. *Chemical Reviews* **2017**, *117*, 4248–4286, doi:10.1021/acs.chemrev.6b00595.
63. El-Sayed, A.; Borghetti, P.; Goiri, E.; Rogero, C.; Floreano, L.; Lovat, G.; Mowbray, D.J.; Cabellos, J.L.; Wakayama, Y.; Rubio, A.; et al. Understanding Energy-Level Alignment in Donor–Acceptor/Metal Interfaces from Core-Level Shifts. *ACS Nano* **2013**, *7*, 6914–6920, doi:10.1021/nn4020888.
64. Taucher, T.C.; Hehn, I.; Hofmann, O.T.; Zharnikov, M.; Zojer, E. Understanding Chemical versus Electrostatic Shifts in X-ray Photoelectron Spectra of Organic Self-Assembled Monolayers. *The Journal of Physical Chemistry C* **2016**, *120*, 3428–3437, doi:10.1021/acs.jpcc.5b12387.
65. Cabarcos, O.M.; Schuster, S.; Hehn, I.; Zhang, P.P.; Maitani, M.M.; Sullivan, N.; Giguère, J.-B.; Morin, J.-F.; Weiss, P.S.; Zojer, E.; et al. Effects of Embedded Dipole Layers on Electrostatic Properties of Alkanethiolate Self-Assembled Monolayers. *The Journal of Physical Chemistry C* **2017**, *121*, 15815–15830, doi:10.1021/acs.jpcc.7b04694.

Preprints (www.preprints.org) | NOT PEER-REVIEWED | Posted: 19 July 2020 doi:10.20944/preprints202007.0406.v1

Peer-reviewed version available at Appl. Sci. 2020, 10, 5735; doi:10.3390/app10175735

66. Siegbahn, K. *ESCA. Atomic, Molecular and Solid State Structure Studied by Means of Electron Spectroscopy. By Kai Siegbahn [and Others], Etc. [With Illustrations.].*; Nova acta Regiae Societatis Scientiarum Upsaliensis. ser. 4. vol. 20; 1967;
67. Benesh, G.A.; King, D.A. Core-level shift spectroscopy for adsorbates: ionic, covalent or metallic bonding? *Chemical Physics Letters* **1992**, *191*, 315–319, doi:10.1016/0009-2614(92)85307-V.
68. Bagus, P.S.; Ilton, E.S.; Nelin, C.J. The interpretation of XPS spectra: Insights into materials properties. *Surface Science Reports* **2013**, *68*, 273–304, doi:10.1016/j.surfrep.2013.03.001.
69. Bagus, P.S.; Ilton, E.; Nelin, C.J. Extracting Chemical Information from XPS Spectra: A Perspective. *Catal Lett* **2018**, *148*, 1785–1802, doi:10.1007/s10562-018-2417-1.
70. Ulman, A. Formation and Structure of Self-Assembled Monolayers. *Chemical Reviews* **1996**, *96*, 1533–1554, doi:10.1021/cr9502357.
71. Schreiber, F. Structure and growth of self-assembling monolayers. *Progress in Surface Science* **2000**, *65*, 151–257, doi:10.1016/S0079-6816(00)00024-1.
72. Heister, K.; Zharnikov, M.; Grunze, M.; Johansson, L.S.O. Adsorption of Alkanethiols and Biphenylthiols on Au and Ag Substrates: A High-Resolution X-ray Photoelectron Spectroscopy Study. *The Journal of Physical Chemistry B* **2001**, *105*, 4058–4061, doi:10.1021/jp010127q.
73. Love, J.C.; Estroff, L.A.; Kriebel, J.K.; Nuzzo, R.G.; Whitesides, G.M. Self-Assembled Monolayers of Thiolates on Metals as a Form of Nanotechnology. *Chemical Reviews* **2005**, *105*, 1103–1170, doi:10.1021/cr0300789.
74. Shaporenko, A.; Cyganik, P.; Buck, M.; Terfort, A.; Zharnikov, M. Self-Assembled Monolayers of Aromatic Selenolates on Noble Metal Substrates. *J. Phys. Chem. B* **2005**, *109*, 13630–13638, doi:10.1021/jp050731r.
75. Käfer, D.; Bashir, A.; Witte, G. Interplay of Anchoring and Ordering in Aromatic Self-Assembled Monolayers. *The Journal of Physical Chemistry C* **2007**, *111*, 10546–10551, doi:10.1021/jp073010w.
76. Merzlikin, S.V.; Tolkachev, N.N.; Strunskus, T.; Witte, G.; Glogowski, T.; Wöll, C.; Grünert, W. Resolving the depth coordinate in photoelectron spectroscopy – Comparison of excitation energy variation vs. angular-resolved XPS for the analysis of a self-assembled monolayer model system. *Surface Science* **2008**, *602*, 755–767, doi:10.1016/j.susc.2007.12.005.
77. Beccari, M.; Kanjilal, A.; Betti, M.G.; Mariani, C.; Floreano, L.; Cossaro, A.; Di Castro, V. Characterization of benzenethiolate self-assembled monolayer on Cu(100) by XPS and NEXAFS. *Journal of Electron Spectroscopy and Related Phenomena* **2009**, *172*, 64–68, doi:10.1016/j.elspec.2009.03.004.
78. Vericat, C.; Vela, M.E.; Benitez, G.; Carro, P.; Salvarezza, R.C. Self-assembled monolayers of thiols and dithiols on gold: new challenges for a well-known system. *Chemical Society Reviews* **2010**, *39*, 1805, doi:10.1039/b907301a.
79. Zaba, T.; Noworolska, A.; Bowers, C.M.; Breiten, B.; Whitesides, G.M.; Cyganik, P. Formation of Highly Ordered Self-Assembled Monolayers of Alkynes on Au(111) Substrate. *J. Am. Chem. Soc.* **2014**, *136*, 11918–11921, doi:10.1021/ja506647p.

Preprints (www.preprints.org) | NOT PEER-REVIEWED | Posted: 19 July 2020 doi:10.20944/preprints202007.0406.v1

Peer-reviewed version available at Appl. Sci. 2020, 10, 5735; doi:10.3390/app10175735

80. Euti, E.M.; Vélez Romero, P.; Linarez Pérez, O.; Ruano, G.; Patrito, E.M.; Zampieri, G.; Leiva, E.P.M.; Macagno, V.A.; Cometto, F.P. Electrochemical, HR-XPS and SERS study of the self-assembly of biphenyl 4,4′-dithiol on Au(111) from solution phase. *Surface Science* **2014**, *630*, 101–108, doi:10.1016/j.susc.2014.07.021.
81. Ossowski, J.; Nascimbeni, G.; Żaba, T.; Verwüster, E.; Rysz, J.; Terfort, A.; Zharnikov, M.; Zojer, E.; Cyganik, P. Relative Thermal Stability of Thiolate- and Selenolate-Bonded Aromatic Monolayers on the Au(111) Substrate. *J. Phys. Chem. C* **2017**, *121*, 28031–28042, doi:10.1021/acs.jpcc.7b09685.
82. Kang, J.F.; Liao, S.; Jordan, R.; Ulman, A. Mixed Self-assembled Monolayers of Rigid Biphenyl Thiols: Impact of Solvent and Dipole Moment. *J. Am. Chem. Soc.* **1998**, *120*, 9662–9667, doi:10.1021/ja981187l.
83. Rong, H.-T.; Frey, S.; Yang, Y.-J.; Zharnikov, M.; Buck, M.; Wühn, M.; Wöll, C.; Helmchen, G. On the Importance of the Headgroup Substrate Bond in Thiol Monolayers: A Study of Biphenyl-Based Thiols on Gold and Silver. *Langmuir* **2001**, *17*, 1582–1593, doi:10.1021/la0014050.
84. Azzam, W.; Fuxen, C.; Birkner, A.; Rong, H.-T.; Buck, M.; Wöll, C. Coexistence of Different Structural Phases in Thioaromatic Monolayers on Au(111). *Langmuir* **2003**, *19*, 4958–4968, doi:10.1021/la020868y.
85. Shaporenko, A.; Terfort, A.; Grunze, M.; Zharnikov, M. A detailed analysis of the photoemission spectra of basic thioaromatic monolayers on noble metal substrates. *Journal of Electron Spectroscopy and Related Phenomena* **2006**, *151*, 45–51, doi:10.1016/j.elspec.2005.10.008.
86. Cyganik, P.; Buck, M.; Strunskus, T.; Shaporenko, A.; Wilton-Ely, J.D.E.T.; Zharnikov, M.; Wöll, C. Competition as a Design Concept: Polymorphism in Self-Assembled Monolayers of Biphenyl-Based Thiols. *J. Am. Chem. Soc.* **2006**, *128*, 13868–13878, doi:10.1021/ja0640647.
87. Stoycheva, S.; Himmelhaus, M.; Fick, J.; Korniakov, A.; Grunze, M.; Ulman, A. Spectroscopic Characterization of ω-Substituted Biphenylthiolates on Gold and Their Use as Substrates for "On-Top" Siloxane SAM Formation. *Langmuir* **2006**, *22*, 4170–4178, doi:10.1021/la0531188.
88. Krzykawska, A.; Ossowski, J.; Żaba, T.; Cyganik, P. Binding groups for highly ordered SAM formation: carboxylic versus thiol. *Chem. Commun.* **2017**, *53*, 5748–5751, doi:10.1039/C7CC01939D.
89. Blum, V.; Gehrke, R.; Hanke, F.; Havu, P.; Havu, V.; Ren, X.; Reuter, K.; Scheffler, M. Ab initio molecular simulations with numeric atom-centered orbitals. *Computer Physics Communications* **2009**, *180*, 2175–2196, doi:10.1016/j.cpc.2009.06.022.
90. Havu, V.; Blum, V.; Havu, P.; Scheffler, M. Efficient integration for all-electron electronic structure calculation using numeric basis functions. *Journal of Computational Physics* **2009**, *228*, 8367–8379, doi:10.1016/j.jcp.2009.08.008.
91. Marek, A.; Blum, V.; Johanni, R.; Havu, V.; Lang, B.; Auckenthaler, T.; Heinecke, A.; Bungartz, H.-J.; Lederer, H. The ELPA library: scalable parallel eigenvalue solutions for electronic structure theory and computational science. *J. Phys.: Condens. Matter* **2014**, *26*, 213201, doi:10.1088/0953-8984/26/21/213201.

Preprints (www.preprints.org) | NOT PEER-REVIEWED | Posted: 19 July 2020 doi:10.20944/preprints202007.0406.v1

Peer-reviewed version available at Appl. Sci. 2020, 10, 5735; doi:10.3390/app10175735

92. Togo, A.; Tanaka, I. Spglib: a software library for crystal symmetry search. *arXiv:1808.01590 [cond-mat]* **2018**.
93. Yu, V.W.; Corsetti, F.; García, A.; Huhn, W.P.; Jacquelin, M.; Jia, W.; Lange, B.; Lin, L.; Lu, J.; Mi, W.; et al. ELSI: A unified software interface for Kohn–Sham electronic structure solvers. *Computer Physics Communications* **2018**, *222*, 267–285, doi:10.1016/j.cpc.2017.09.007.
94. Perdew, J.P.; Burke, K.; Ernzerhof, M. Generalized Gradient Approximation Made Simple. *Physical Review Letters* **1996**, *77*, 3865–3868, doi:10.1103/PhysRevLett.77.3865.
95. Perdew, J.P.; Burke, K.; Ernzerhof, M. ERRATA: Generalized Gradient Approximation Made Simple [Phys. Rev. Lett. 77, 3865 (1996)]. *Physical Review Letters* **1997**, *78*, 1396–1396, doi:10.1103/PhysRevLett.78.1396.
96. Ruiz, V.G.; Liu, W.; Zojer, E.; Scheffler, M.; Tkatchenko, A. Density-Functional Theory with Screened van der Waals Interactions for the Modeling of Hybrid Inorganic-Organic Systems. *Physical Review Letters* **2012**, *108*, doi:10.1103/PhysRevLett.108.146103.
97. Tkatchenko, A.; Scheffler, M. Accurate Molecular Van Der Waals Interactions from Ground-State Electron Density and Free-Atom Reference Data. *Physical Review Letters* **2009**, *102*, doi:10.1103/PhysRevLett.102.073005.
98. Neugebauer, J.; Scheffler, M. Adsorbate-substrate and adsorbate-adsorbate interactions of Na and K adlayers on Al(111). *Physical Review B* **1992**, *46*, 16067–16080, doi:10.1103/PhysRevB.46.16067.
99. Freysoldt, C.; Eggert, P.; Rinke, P.; Schindlmayr, A.; Scheffler, M. Screening in two dimensions: G W calculations for surfaces and thin films using the repeated-slab approach. *Phys. Rev. B* **2008**, *77*, 235428, doi:10.1103/PhysRevB.77.235428.
100. Verwüster, E.; Hofmann, O.T.; Egger, D.A.; Zojer, E. Electronic Properties of Biphenylthiolates on Au(111): The Impact of Coverage Revisited. *The Journal of Physical Chemistry C* **2015**, *119*, 7817–7825, doi:10.1021/acs.jpcc.5b00992.
101. Vackář, J.; Hyt'ha, M.; Šimůnek, A. All-electron pseudopotentials. *Physical Review B* **1998**, *58*, 12712–12720, doi:10.1103/PhysRevB.58.12712.
102. Methfessel, M.; Fiorentini, V.; Oppo, S. Connection between charge transfer and alloying core-level shifts based on density-functional calculations. *Phys. Rev. B* **2000**, *61*, 5229–5236, doi:10.1103/PhysRevB.61.5229.
103. Morikawa, Y.; Hayashi, T.; Liew, C.C.; Nozoye, H. First-principles theoretical study of alkylthiolate adsorption on Au (111). *Surface science* **2002**, *507*, 46–50.
104. Heimel, G.; Romaner, L.; Brédas, J.-L.; Zojer, E. Organic/metal interfaces in self-assembled monolayers of conjugated thiols: A first-principles benchmark study. *Surface Science* **2006**, *600*, 4548–4562, doi:10.1016/j.susc.2006.07.023.
105. Giesbers, M.; Marcelis, A.T.M.; Zuilhof, H. Simulation of XPS C1s Spectra of Organic Monolayers by Quantum Chemical Methods. *Langmuir* **2013**, *29*, 4782–4788, doi:10.1021/la400445s.

Preprints (www.preprints.org) | NOT PEER-REVIEWED | Posted: 19 July 2020 doi:10.20944/preprints202007.0406.v1

Peer-reviewed version available at Appl. Sci. 2020, 10, 5735; doi:10.3390/app10175735

106. Pueyo Bellafont, N.; Illas, F.; Bagus, P.S. Validation of Koopmans' theorem for density functional theory binding energies. *Phys. Chem. Chem. Phys.* **2015**, *17*, 4015–4019, doi:10.1039/C4CP05434B.
107. Ishiwari, F.; Nascimbeni, G.; Sauter, E.; Tago, H.; Shoji, Y.; Fujii, S.; Kiguchi, M.; Tada, T.; Zharnikov, M.; Zojer, E.; et al. Triptycene Tripods for the Formation of Highly Uniform and Densely Packed Self-Assembled Monolayers with Controlled Molecular Orientation. *J. Am. Chem. Soc.* **2019**, *141*, 5995–6005, doi:10.1021/jacs.9b00950.
108. Sauter, E.; Nascimbeni, G.; Trefz, D.; Ludwigs, S.; Zojer, E.; Wrochem, F. von; Zharnikov, M. A dithiocarbamate anchoring group as a flexible platform for interface engineering. *Phys. Chem. Chem. Phys.* **2019**, *21*, 22511–22525, doi:10.1039/C9CP03306H.
109. Pueyo Bellafont, N.; Bagus, P.S.; Illas, F. Prediction of core level binding energies in density functional theory: Rigorous definition of initial and final state contributions and implications on the physical meaning of Kohn-Sham energies. *The Journal of Chemical Physics* **2015**, *142*, 214102, doi:10.1063/1.4921823.
110. Viñes, F.; Sousa, C.; Illas, F. On the prediction of core level binding energies in molecules, surfaces and solids. *Phys. Chem. Chem. Phys.* **2018**, *20*, 8403–8410, doi:10.1039/C7CP08503F.
111. Kirchhuebel, T.; Monti, O.L.A.; Munakata, T.; Kera, S.; Forker, R.; Fritz, T. The role of initial and final states in molecular spectroscopies. *Phys. Chem. Chem. Phys.* **2019**, *21*, 12730–12747, doi:10.1039/C8CP07318J.
112. Taucher, T.C.; Hofmann, O.T.; Zojer, E. Final-State Simulations of Core-Level Binding Energies at Metal-Organic Hybrid Interfaces: Artifacts Caused by Spurious Collective Electrostatic Effects. *submitted* **2020**.
113. Jackson, J.D. *Classical electrodynamics*; 3rd ed.; Wiley: New York, 1999; ISBN 978-0-471-30932-1.
114. Neaton, J.B.; Hybertsen, M.S.; Louie, S.G. Renormalization of Molecular Electronic Levels at Metal-Molecule Interfaces. *Phys. Rev. Lett.* **2006**, *97*, 216405, doi:10.1103/PhysRevLett.97.216405.
115. Lamont, C.L.; Wilkes, J. Attenuation length of electrons in self-assembled monolayers of n-alkanethiols on gold. *Langmuir* **1999**, *15*, 2037–2042.
116. van der Walt, S.; Colbert, S.C.; Varoquaux, G. The NumPy Array: A Structure for Efficient Numerical Computation. *Comput. Sci. Eng.* **2011**, *13*, 22–30, doi:10.1109/MCSE.2011.37.
117. Hunter, J.D. Matplotlib: A 2D Graphics Environment. *Comput. Sci. Eng.* **2007**, *9*, 90–95, doi:10.1109/MCSE.2007.55.
118. Stukowski, A. Visualization and analysis of atomistic simulation data with OVITO–the Open Visualization Tool. *Modelling and Simulation in Materials Science and Engineering* **2010**, *18*, 015012, doi:10.1088/0965-0393/18/1/015012.
119. Momma, K.; Izumi, F. *VESTA 3* for three-dimensional visualization of crystal, volumetric and morphology data. *J Appl Crystallogr* **2011**, *44*, 1272–1276, doi:10.1107/S0021889811038970.

Preprints (www.preprints.org) | NOT PEER-REVIEWED | Posted: 19 July 2020 doi:10.20944/preprints202007.0406.v1

Peer-reviewed version available at Appl. Sci. 2020, 10, 5735; doi:10.3390/app10175735

120. The GIMP Development Team *GIMP*; 2019;
121. Sze, S.M.; Ng, K.K. *Physics of semiconductor devices*; 3rd ed.; Wiley-Interscience: Hoboken, N.J, 2007; ISBN 978-0-471-14323-9.
122. Stähler, J.; Rinke, P. Global and local aspects of the surface potential landscape for energy level alignment at organic-ZnO interfaces. *Chemical Physics* **2017**, *485–486*, 149–165, doi:10.1016/j.chemphys.2016.11.017.
123. Heimel, G.; Rissner, F.; Zojer, E. Modeling the Electronic Properties of π-Conjugated Self-Assembled Monolayers. *Advanced Materials* **2010**, *22*, 2494–2513, doi:10.1002/adma.200903855.
124. Natan, A.; Zidon, Y.; Shapira, Y.; Kronik, L. Cooperative effects and dipole formation at semiconductor and self-assembled-monolayer interfaces. *Physical Review B* **2006**, *73*, doi:10.1103/PhysRevB.73.193310.
125. Egelhoff, W.F. Core-level binding-energy shifts at surfaces and in solids. *Surface Science Reports* **1987**, *6*, 253–415, doi:https://doi.org/10.1016/0167-5729(87)90007-0.
126. Bagus, P.S.; Nelin, C.J.; Zhao, X.; Levchenko, S.V.; Davis, E.; Weng, X.; Späth, F.; Papp, C.; Kuhlenbeck, H.; Freund, H.-J. Revisiting surface core-level shifts for ionic compounds. *Phys. Rev. B* **2019**, *100*, 115419, doi:10.1103/PhysRevB.100.115419.
127. Vericat, C.; Vela, M.E.; Corthey, G.; Pensa, E.; Cortés, E.; Fonticelli, M.H.; Ibañez, F.; Benitez, G.E.; Carro, P.; Salvarezza, R.C. Self-assembled monolayers of thiolates on metals: a review article on sulfur-metal chemistry and surface structures. *RSC Adv.* **2014**, *4*, 27730–27754, doi:10.1039/C4RA04659E.
128. Ma, Z.; Rissner, F.; Wang, L.; Heimel, G.; Li, Q.; Shuai, Z.; Zojer, E. Electronic structure of pyridine-based SAMs on flat Au(111) surfaces: extended charge rearrangements and Fermi level pinning. *Phys. Chem. Chem. Phys.* **2011**, *13*, 9747, doi:10.1039/c0cp02168g.
129. Hofmann, O.T.; Deinert, J.-C.; Xu, Y.; Rinke, P.; Stähler, J.; Wolf, M.; Scheffler, M. Large work function reduction by adsorption of a molecule with a negative electron affinity: Pyridine on ZnO($10\bar{1}0$). *The Journal of Chemical Physics* **2013**, *139*, 174701, doi:10.1063/1.4827017.
130. Hébert, P.; Le Rille, A.; Zheng, W.Q.; Tadjeddine, A. Vibrational spectroscopic study of the adsorption of pyridine at the Au(111)-electrolyte interface by in situ difference frequency generation. *Journal of Electroanalytical Chemistry* **1998**, *447*, 5–9, doi:10.1016/S0022-0728(98)00035-7.
131. Stadler, R.; Thygesen, K.S.; Jacobsen, K.W. Forces and conductances in a single-molecule bipyridine junction. *Phys. Rev. B* **2005**, *72*, 241401, doi:10.1103/PhysRevB.72.241401.
132. Kamenetska, M.; Quek, S.Y.; Whalley, A.C.; Steigerwald, M.L.; Choi, H.J.; Louie, S.G.; Nuckolls, C.; Hybertsen, M.S.; Neaton, J.B.; Venkataraman, L. Conductance and Geometry of Pyridine-Linked Single-Molecule Junctions. *J. Am. Chem. Soc.* **2010**, *132*, 6817–6821, doi:10.1021/ja1015348.

Preprints (www.preprints.org) | NOT PEER-REVIEWED | Posted: 19 July 2020 doi:10.20944/preprints202007.0406.v1

Peer-reviewed version available at Appl. Sci. 2020, 10, 5735; doi:10.3390/app10175735

133. Obersteiner, V.; Egger, D.A.; Zojer, E. Impact of Anchoring Groups on Ballistic Transport: Single Molecule vs Monolayer Junctions. *The Journal of Physical Chemistry C* **2015**, *119*, 21198–21208, doi:10.1021/acs.jpcc.5b06110.
134. Smith, C.E.; Xie, Z.; Bâldea, I.; Frisbie, C.D. Work function and temperature dependence of electron tunneling through an N-type perylene diimide molecular junction with isocyanide surface linkers. *Nanoscale* **2018**, *10*, 964–975, doi:10.1039/C7NR06461F.
135. Tsunoi, A.; Lkhamsuren, G.; Mondarte, E.A.Q.; Asatyas, S.; Oguchi, M.; Noh, J.; Hayashi, T. Improvement of the Thermal Stability of Self-Assembled Monolayers of Isocyanide Derivatives on Gold. *J. Phys. Chem. C* **2019**, *123*, 13681–13686, doi:10.1021/acs.jpcc.9b02256.
136. Bagus, P.S.; Staemmler, V.; Wöll, C. Exchangelike Effects for Closed-Shell Adsorbates: Interface Dipole and Work Function. *Physical Review Letters* **2002**, *89*, doi:10.1103/PhysRevLett.89.096104.
137. Mizushima, H.; Koike, H.; Kuroda, K.; Ishida, Y.; Nakayama, M.; Mase, K.; Kondo, T.; Shin, S.; Kanai, K. Effect of physisorption of inert organic molecules on Au(111) surface electronic states. *Physical Chemistry Chemical Physics* **2017**, *19*, 18646–18651, doi:10.1039/C7CP04232A.
138. Macdonald, J.R.; Barlow, C.A. Work Function Change on Monolayer Adsorption. *J. Chem. Phys.* **1963**, *39*, 412–422, doi:10.1063/1.1734263.
139. Maschhoff, B.L.; Cowin, J.P. Corrected electrostatic model for dipoles adsorbed on a metal surface. *J. Chem. Phys.* **1994**, *101*, 8138–8151, doi:10.1063/1.468241.
140. Gershevitz, O.; Sukenik, C.N.; Ghabboun, J.; Cahen, D. Molecular Monolayer-Mediated Control over Semiconductor Surfaces: Evidence for Molecular Depolarization of Silane Monolayers on Si/SiOx. *J. Am. Chem. Soc.* **2003**, *125*, 4730–4731, doi:10.1021/ja029529h.
141. De Renzi, V.; Rousseau, R.; Marchetto, D.; Biagi, R.; Scandolo, S.; del Pennino, U. Metal Work-Function Changes Induced by Organic Adsorbates: A Combined Experimental and Theoretical Study. *Phys. Rev. Lett.* **2005**, *95*, 046804, doi:10.1103/PhysRevLett.95.046804.
142. Fukagawa, H.; Yamane, H.; Kera, S.; Okudaira, K.K.; Ueno, N. Experimental estimation of the electric dipole moment and polarizability of titanyl phthalocyanine using ultraviolet photoelectron spectroscopy. *Phys. Rev. B* **2006**, *73*, 041302, doi:10.1103/PhysRevB.73.041302.
143. Cornil, D.; Olivier, Y.; Geskin, V.; Cornil, J. Depolarization Effects in Self-Assembled Monolayers: A Quantum-Chemical Insight. *Advanced Functional Materials* **2007**, *17*, 1143–1148, doi:10.1002/adfm.200601116.
144. Sushko, M.L.; Shluger, A.L. Intramolecular Dipole Coupling and Depolarization in Self-Assembled Monolayers. *Advanced Functional Materials* **2008**, *18*, 2228–2236, doi:10.1002/adfm.200701305.
145. Piacenza, M.; D'Agostino, S.; Fabiano, E.; Della Sala, F. Ab initio depolarization in self-assembled molecular monolayers: Beyond conventional density-functional theory. *Phys. Rev. B* **2009**, *80*, 153101, doi:10.1103/PhysRevB.80.153101.

Preprints (www.preprints.org) | NOT PEER-REVIEWED | Posted: 19 July 2020 doi:10.20944/preprints202007.0406.v1

Peer-reviewed version available at Appl. Sci. 2020, 10, 5735; doi:10.3390/app10175735

146. Blumenfeld, M.L.; Steele, M.P.; Monti, O.L.A. Near- and Far-Field Effects on Molecular Energy Level Alignment at an Organic/Electrode Interface. *J. Phys. Chem. Lett.* **2010**, *1*, 145–148, doi:10.1021/jz9000517.
147. Wang, L.; Rangger, G.M.; Romaner, L.; Heimel, G.; Bučko, T.; Ma, Z.; Li, Q.; Shuai, Z.; Zojer, E. Electronic Structure of Self-Assembled Monolayers on Au(111) Surfaces: The Impact of Backbone Polarizability. *Advanced Functional Materials* **2009**, *19*, 3766–3775, doi:10.1002/adfm.200901152.
148. Koller, G.; Winter, B.; Oehzelt, M.; Ivanco, J.; Netzer, F.P.; Ramsey, M.G. The electronic band alignment on nanoscopically patterned substrates. *Organic Electronics* **2007**, *8*, 63–68, doi:10.1016/j.orgel.2006.11.001.